ACS APPLIED MATERIALS & INTERFACES

Research Article

www.acsami.org

Red-Emitting DPSB-Based Conjugated Polymer Nanoparticles with High Two-Photon Brightness for Cell Membrane Imaging

Peng Liu,[†,‡] Shuang Li,[‡] Yaocheng Jin,[†] Linghui Qian,[‡] Nengyue Gao,[‡] Shao Q. Yao,[‡] Fei Huang,*[,†] Qing-Hua Xu,*[,‡] and Yong Cao[†]

[†]Institute of Polymer Optoelectronic Materials and Devices, State Key Laboratory of Luminescent Materials and Devices, South China University of Technology, Guangzhou 510640, P. R. China

[‡]Department of Chemistry, National University of Singapore,3 Science Drive 3, Singapore117543

Supporting Information

ABSTRACT: New red-emitting conjugated polymers have been successfully synthesized by incorporating classical two-photon absorption (TPA) units, electron-rich units, and a small amount of electron-deficient units along the polymer backbones. Water-dispersible nanoparticles (NPs) based on these polymers were also fabricated for applications in two-photon excitation fluorescence imaging of cell membrane. Through optimization of the polymer/matrix mass ratio and the initial feed concentration of the polymer solution, a high quantum yield (QY) of 24% was achieved for the red-emitting NPs in water. TPA cross section and two-photon action cross section values of these polymers at 750 nm reached up to 1000 GM and 190 GM per repeat unit in aqueous media, 2.5×10^5 GM and 4.7×10^4 GM per NP, respectively. Furthermore, these NPs displayed excellent photostability and biocompatibility. Their applications as two-photon excitation fluorescence probes for cell membrane imaging have been demonstrated in three different cell lines with excellent imaging contrast. These results demonstrated that these polymer NPs hold great potentials as excellent two-photon excitation fluorescence probes in various biological applications.

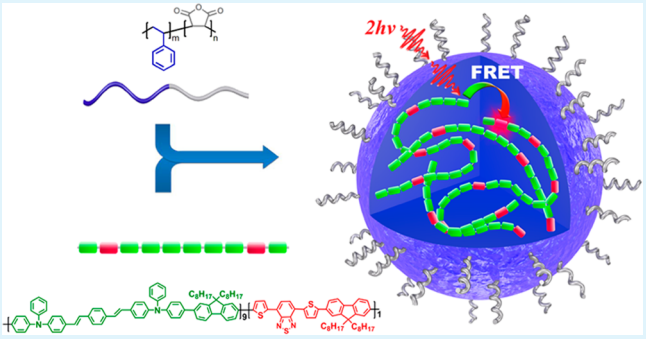

KEYWORDS: *conjugated polymers, nanoparticles, energy transfer, two-photon, fluorescence, cell imaging*

INTRODUCTION

As a noninvasive intravital imaging technique on the single-cell level, two-photon excitation (2PE) fluorescence imaging has attracted great research interest for investigating complex biological and physiological events in the past decade.[1−5] Compared with conventional one-photon excitation fluorescence imaging, 2PE fluorescence imaging possesses unique advantages, such as deeper tissue penetration, lower autofluorescence, less photobleaching and reduced phototoxicity, because of the use of near-infrared (700−1000 nm) excitation source and quadratic dependence of two-photon absorption probability on the incident light intensity.[6−9] Various fluorescent materials, including small organic dyes,[10] fluorescent proteins,[11] and inorganic semiconductor quantum dots (QDs),[12] have been employed as the probes for 2PE fluorescence imaging. However, all these materials suffer from some drawbacks, such as poor photostability of organic dyes and proteins,[13] high toxicity, and irregular blinking behaviors of QDs.[14] As a class of macromolecule consisting of delocalized π-electrons along the polymer backbone, conjugated polymers (CPs) exhibit large extinction coefficients, high fluorescence quantum yields, good photostability, and biocompatibility.[15,16]

To be useful for biological applications, water solubility of hydrophobic CPs was improved either by chemical modification with the ionic side chains (i.e., the polyelectrolytes)[17] or physical approach via emulsion or reprecipitation to fabricate water-dispersible nanoparticles.[18−21] CP nanoparticles (NPs) with emission spanning the full range of the visible spectrum have been developed owing to the facile fine-tuning of the conjugation structures.[22−24] Far-red/near-infrared (FR/NIR) emitting NPs are important for bioimaging because of their deep tissue penetration for efficient emission detection.[25−27] However, red emitters generally have planar aromatic structures, which make them easy to aggregate in aqueous media via $\pi-\pi$ stacking and hydrophobic interactions, leading to significantly reduced fluorescence quantum yield (QY).[24,28] To mitigate the aggregation effect and obtain larger Stokes shift, physical blending CPs with NIR fluorescent acceptors[29−31] and chemical introduction of narrow-band gap moieties into CP backbones[32,33] are generally utilized to obtain NPs that emit in the FR or NIR range. In these methods, donor

Received: January 8, 2015
Accepted: March 12, 2015
Published: March 12, 2015

DOI: 10.1021/acsami.5b00223
ACS Appl. Mater. Interfaces 2015, 7, 6754−6763

(D) and acceptor (A) molecules are encapsulated into the NP matrix, in which excitation energy is transferred from the donor to the acceptor through fluorescence resonance energy transfer (FRET),[25,34,35] leading to large apparent Stokes shift. Compared with sophisticated chemical modification of the fluorophores, FRET strategy is more straightforward and flexible. Ideal two-photon chromophores need to have high QY (η) and large TPA cross section (δ). The product of both was defined as two-photon action cross section ($\eta\delta$), which determines two-photon brightness and better signal-to-noise ratio to achieve high contrast images.[36−38] Various strategies for construction of the molecules with large TPA cross sections have been explored. Dyes with extended π-conjugated systems symmetrically substituted with electron-donating or accepting functional groups have been known to display large δ values. δ values could be improved by optimizing many factors, such as conjugation length, molecular planarity, intramolecular charge transfer, vibronic coupling, dimensionality of the charge-transfer network, and the electron donating and withdrawing abilities of the donor and acceptor.[21,39−43] However, $\eta\delta$ values of most TPA molecules decrease significantly when transferred from organic solvent into polar aqueous media because of aggregation, which could be overcome by using amphiphilic block polymers as the encapsulation matrix.[44,45]

Two-photon chromophores based on the structure of bis(diphenylaminostyryl)benzene (DPSB) have been demonstrated to possess efficient D-π-D structures with large δ values (Scheme 1).[42,46−48] Herein we designed and synthesized a series of DPSB based conjugated polymers (Scheme 1). Linearly copolymer M1 and cross-copolymer S1 were synthesized by copolymerization of DPSB units and fluorene units. Dithienylbenzothiadiazole (DTBT) units were further introduced into the backbones to act as energy acceptor to redshift the emission wavelength to far-red range and form a D-π-A-π-D structure to improve their TPA cross sections (M2 and S2). Water dispersible NPs based on these polymers were prepared by using poly(styrene-*co*-maleic anhydride) (PSMA) as the encapsulation matrix. These NPs were further optimized by adjusting the polymer/matrix mass ratio and the initial feed concentration of the polymers. Applications of these CP NPs as two-photon fluorescence probes for cell membrane imaging were subsequently demonstrated.

Scheme 1. (a) Chemical Structures of DPSB, Encapsulation Matrix PSMA, and Polymer S1, S2, M1, M2 and (b) Illustrative Preparation Procedures of Conjugated Polymer NPs

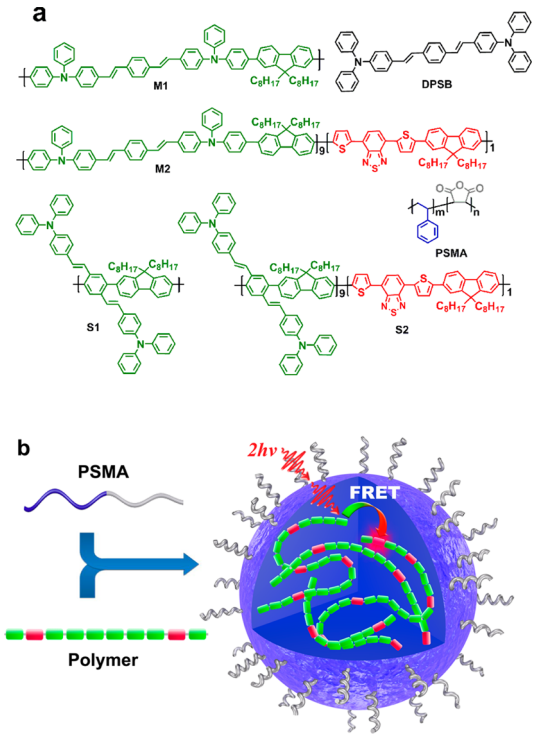

RESULTS AND DISCUSSION

Synthesis and Characterization. Scheme 2 shows the synthesis routes of the four conjugated polymers (the detailed synthetic routes of the monomers are shown in Figure S1 in the Supporting Information). Monomers 3a and 3b were synthesized via a Horner−Emmons reaction between phosphoric acid diethylester and diphenylaminobenzaldehyde. The polymers (M1, M2, S1, and S2) were synthesized by Suzuki polymerization at 85 °C. M2 and S2 were prepared by incorporating 5.0 mol % of electron accepting unit, DTBT, into the polymer backbones, which was an optimum ratio for efficient energy transfer in the NPs. The reaction times for M1 and M2 (2−3 h) were much shorter than those for S1 and S2 (24 h) to prevent gel formation during the reaction, which was due to their relatively lower solubility, especially for M1. The solubility differences can be attributed to more extended π-electron conjugation systems and higher chain planarity of M1 and M2 compared to S1 and S2. M1 and M2 exhibited smaller molecular weights than those of S1and S2 due to short reaction times. Water dispersible NPs were prepared by using a reprecipitation method with and without PSMA as the encapsulation matrix (PSMA-CP and bare-CP NPs, CP denotes S1, S2, M1and M2). The morphologies and sizes of the PSMA-CP NPs were characterized by transmission electron microscopy (TEM) and dynamic light scattering (DLS) measurements. Average diameter of 23 nm was obtained for PSMA-M2 NPs from TEM measurement (Figure 1a), consistent with the DLS results (Figure 1b, 26 nm). The

Scheme 2. Synthetic Routes for S1, S2, M1, and M2

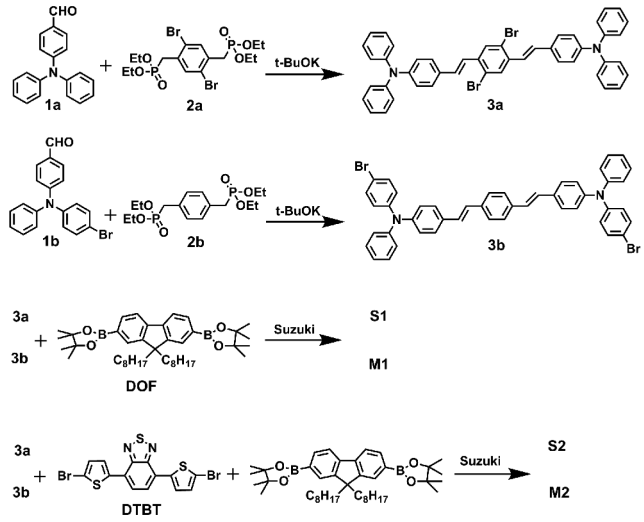

DOI: 10.1021/acsami.5b00223
ACS Appl. Mater. Interfaces 2015, 7, 6754−6763

results of other CP NPs are shown in the Supporting Information (Figures S2 and S3).

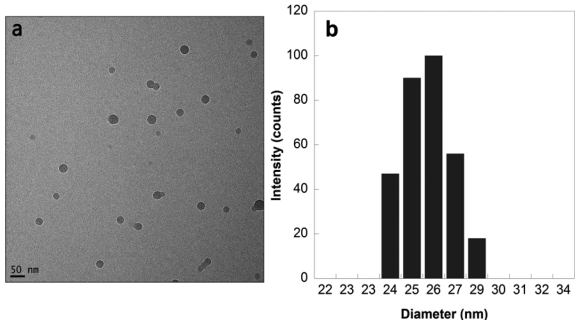

Figure 1. TEM image (a) and DLS distribution (b) of PSMA-M2 NPs.

Absorption and Fluorescence Properties. Absorption and fluorescence spectra of four conjugated polymers (M1, M2, S1 and S2) in tetrahydrofuran (THF) and NP dispersion in water are shown in Figure 2. M1 and M2 showed larger molar

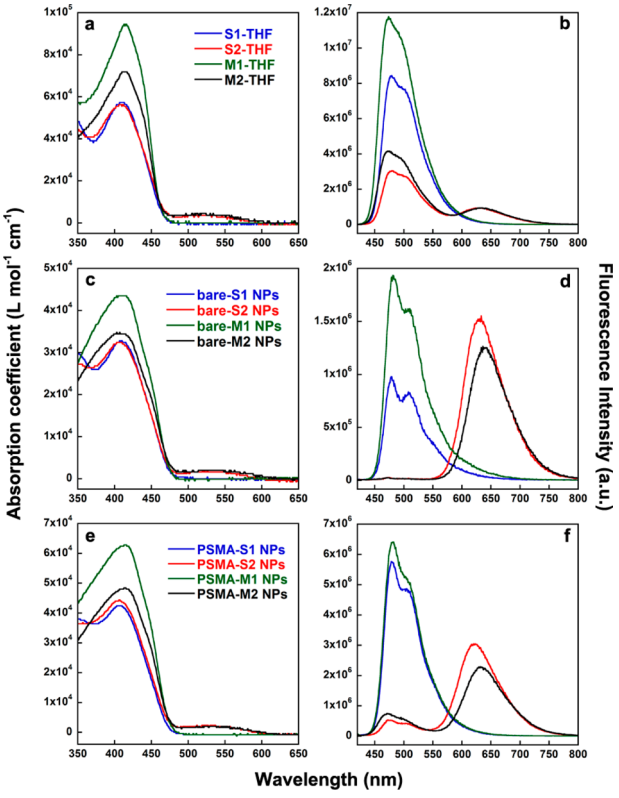

Figure 2. Absorption (left) and fluorescence spectra (right, λ_{EX} = 410 nm) of M1, M2, S1, and S2 in THF (a, b, 1.0 μM), bare-CP NPs in water (c, d, 2.5 μM), and PSMA-CP NPs in water (e, f, 2.5 μM).

extinction coefficients (per RU) than S1 and S2, which can be ascribed to reduced planarity of the π-electron conjugation systems in S1 and S2.[49] In THF solution, the polymers exist in a "molecularly dissolved" state. M1 and M2 THF solutions exhibited dominant absorption peaks at 415 nm, which were ~5 nm red-shifted compared to those of S1 and S2 due to larger π-conjugation length. The CP NP dispersions in water (bare-NPs and PSMA-NPs) displayed slightly broadened and ~5 nm blue-shifted absorption spectra compared to those in THF solution. The observed blue-shift in absorption spectra reflects decreased conjugation length due to bending, torsion and kinking of the polymer backbones inside the nanoparticles.[50] Fluorescence spectra of M2/S2 THF solution displayed a dominant donor emission band at ~480 nm and a small acceptor emission band at ~630 nm. In bare-NPs, the fluorescence spectra of M2/S2 were dominated by the acceptor emission band at ~630 nm. The energy transfer efficiencies in bare-NPs were found to be nearly 100%, significantly enhanced due to 3-dimensional contacts between the donor and acceptor segments in NPs. The energy transfer efficiencies in PSMA-M2/S2 NPs were slightly reduced due to introduction of PSMA matrix, in which the hydrophobic parts of PSMA interpenetrate with the polymer chains to reduce the contact between the donor and acceptor segments. Although introduction of PSMA slightly reduced the FRET efficiencies, the absolute intensities of the acceptor emission peaks were significantly larger than that of the bare-M2/S2 NPs at the same CP solution concentration. These results suggest that introduction of PSMA helps to improve QY of donor or acceptor segments.

Optimization of Conjugated Polymer NPs. The CP NPs in the aqueous solution were prepared by using an amphiphilic block copolymer, PSMA, as the surfactant and encapsulation matrix. The ratio of CP to surfactant is important for controlling the morphology of CP domains inside the NPs and improving their QYs.[45,51] The initial CP concentration in the precursor solution has also been known to influence the particle size and self-assembly behaviors of CP inside the NPs and consequently their QYs.[18,52]

Figure 3a and b shows fluorescence spectra of PSMA-M1 and PSMA-M2 NPs with mass ratios of CP to PSMA ranging from 1:0 to 1:200, while the CP concentration was kept at 2.5 μM (in RU). The emission intensities of donor and acceptor segments for different PSMA-M1 and PSMA-M2 NPs are summarized in Figure 3c. The results for PSMA-S1 and PSMA-

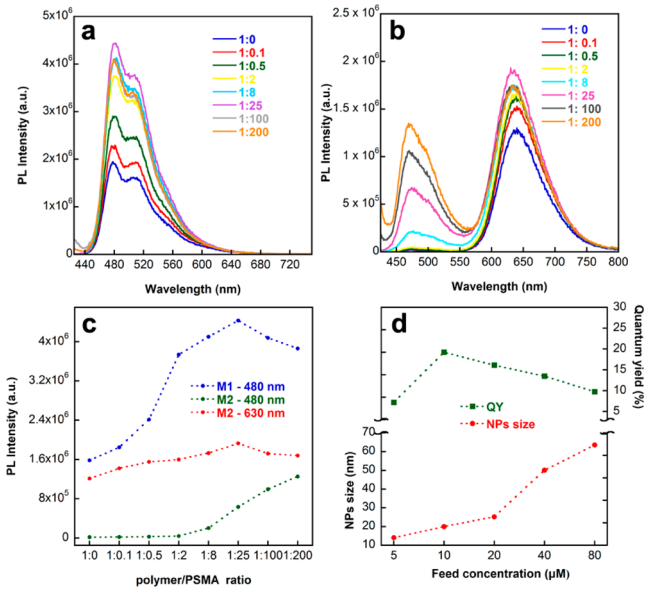

Figure 3. Fluorescence spectra of PSMA-M1 NPs (a) and PSMA-M2 NPs (b) with polymer/PSMA mass ratios varying from 1:0 to 1:200. (c) Fluorescence intensity variation of donor and acceptor emission peaks with different polymer/PSMA mass ratios. (d) QYs and NPs size of the PSMA-M2 NPs prepared from different feed concentrations of polymer in THF. λ_{EX} = 410 nm.

DOI: 10.1021/acsami.5b00223
ACS Appl. Mater. Interfaces 2015, 7, 6754−6763

S2 NPs are summarized in Supporting Information Figure S4. As the PSMA content inside the NPs increased, fluorescence intensity of PSMA-M1 NPs (at 480 nm) increased until reaching an optimum QY of 30% at CP/PSMA mass ratio of 1:25, then slightly decreased at very high PSMA contents because of the surfactant oversaturation caused by excessive PSMA. The oversaturation was indicated by the observation of the NPs solution getting turbid at higher PSMA contents. The donor emission (at 480 nm) and acceptor emission peaks (at 630 nm) of PSMA-M2 NPs both increased steadily with the increasing content of PSMA at first due to the separation effect of PSMA against aggregation induced quenching. After PSMA content increased above the optimum CP/PSMA mass ratio at 1:25, the donor emission peak grew continuously but the acceptor emission peak started to fall, which can be attributed to the reduced FRET efficiency as the excess PSMA increased the donor−acceptor separation distances. The PSMA-S2 NPs were also found to give the largest acceptor emission intensities at CP/PSMA mass ratio of 1:25 (Supporting Information Figure S4).

The effects of initial CP concentration in the precursor solution on the particle size and QY have also been investigated on PSMA-M2 NPs (Figure 3d and Supporting Information Figure S5). As the initial feed concentration of M2 increased from 5.0 to 80 μM (in RU at CP/PSMA mass ratio of 1:25), the particle size increased steadily from 14 to 64 nm (hydrodynamic diameters by DLS). The optimum fluorescence intensity of the acceptor emission band was observed for NPs with diameter of 26 nm prepared by using initial M2 feed concentration of 10 μM. Further higher feed concentration led to slightly decreased donor and acceptor emission intensities and increased acceptor/donor emission intensity ratio. These observations indicated that the chromophores were likely to aggregate inside larger NPs as PSMA surfactants tend to locate at the surface of the NPs and consequently decreased QYs of donors and acceptors for larger NPs despite increased energy transfer efficiency.

High stability in biological environment is critical for in vivo applications of nanoparticles. The stability of these NPs was evaluated by monitoring their fluorescence intensities after incubation with 1 × phosphate buffer solution (PBS) at 37 °C for up to 10 days (Supporting Information Figure S6). It was found that the fluorescence intensities of these polymer NPs remained almost 100% of their initial values after incubation for up to 10 days. In contrast, the commercially available quantum dot, QD655, a widely used labeling agent for two-photon imaging, has been reported to show over 50% decrease in fluorescence intensity under the same condition.[33,53] The photostabilities of PSMA-M2 NPs in aqueous solution (2.5 μM in RU) and spin-coated M2 polymer thin films (50 nm thick) were examined under continuous one-photon excitation at 410 nm (4 mW) and fs laser excitation at 750 nm (100 mW) for 10 min (Figure S7 in the Supporting Information). The fluorescence intensities of PSMA-M2 NPs in aqueous solution remained nearly constant after fs laser illumination for 10 min, while that of M2 polymer thin films (without surfactant protection, the extreme case) decreased by 40% under the same condition. Because of high photon flux and the resonant nature of two-photon excitation, photobleaching is generally unavoidable within the excitation area.[54] As two-photon excitation in laser scanning microscopy restricts excitation to the focal plane and the illumination time at each point is less than 1 ms in a typical cell imaging experiment, the photobleaching effect is minimized and restricted within the small focal volume without photobleaching the sample within the whole illumination area as in the one-photon excitation. These NPs displayed sufficient photostability against photobleaching for in vivo cell imaging experiments despite the high laser power. Moreover, the zeta potential of these NPs remained nearly unchanged after incubation in PBS at 37 °C for up to 10 days(Figure S8 in the Supporting Information), which further confirm their high kinetic stability in the biological environment.

Fluorescence Quantum Yield and Lifetime. Fluorescence QYs of the different samples are summarized in Table 1.

Table 1. Fluorescence Quantum Yields of Different Samples (CP/PSMA Mass Ratio of 1:25 for PSMA-CP NPs)[a]

polymer	THF (%)	bare-CP NPs (%)	PSMA-CP NPs (%)
S1	92	9	32
S2	61(19)	14(14)	27(24)
M1	84	9	30
M2	66(16)	11(11)	23(19)

[a]The QYs in the brackets for S2 and M2 are calculated only from the acceptor emission bands ranging from 550 to 800 nm.

The QYs in the brackets for S2 and M2 are calculated based on the acceptor emission bands ranging from 550 to 800 nm only. Four CPs showed high quantum yields (from 61% to 92%) in the THF solution. The QYs of the corresponding bare NPs in water decreased down to 9−14% because of aggregation-induced quenching. Incorporation of amphiphilic PSMA into PSMA-M1 and PSMA-S1 NPs to separate adjacent conjugated segments helps to mitigate the self-quenching effects and leads to higher QYs. Introduction of PSMA has complicated effects on the red emission of the PSMA-M2 and PSMA-S2 NPs. On the one hand, introduction of PSMA will increase the QY of donor and acceptor segments in overall. On the other hand, too much PSMA will reduce energy transfer efficiency from the donor segments to acceptor segments. An optimum PSMA content is required for the largest red emission intensity (Figure 3).The effective red-emission QYs (550 to 800 nm portion) of PSMA-M2 and PSMA-S2 NPs were found to reach up to 19% and 24%, respectively. This is quite high as red-emitting fluorophores generally have low quantum yields because of small band gaps.

Fluorescence lifetimes of different samples were measured by using a time-correlated single photon counting (TCSPC) method (Figure 4 and Supporting Information Figures S9 and S10 and Tables S1−S4). The spectral resolution was set as 1.0 nm and full-width at half-maximum of the instrument response

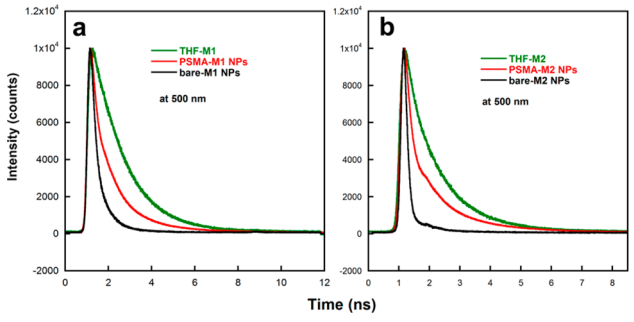

Figure 4. Fluorescence decay curves of M1 (a) and M2 (b) in different states.

DOI: 10.1021/acsami.5b00223
ACS Appl. Mater. Interfaces 2015, 7, 6754−6763

function (IRF) was ~200 ps, which give a temporal resolution of ~100 ps after deconvolution. The TCSPC results (Figure 4) are consistent with steady state fluorescence spectra and quantum yield results. The fluorescence lifetime of M1 samples at 500 nm decreased from its THF solution, to PSMA encapsulated NPs and then to bare NPs (Figure 4a), which is consistent with their decreasing QYs in the corresponding states due to increased aggregation induced self-quenching. The fluorescence lifetime of donor emission at 500 nm of M2 in THF solution, PSMA-M2 NPs and bare M2 NPs are shorter than those of the corresponding M1 samples because of the energy transfer processes in M2 (Figure 4b). The differences in lifetimes between M1 and M2 samples at donor emission peak (500 nm) increased in the order of THF solution, PSMA encapsulated NPs and bare NPs, consistent with increasing energy transfer rates due to the decreasing donor−acceptor separation distances in these samples. Fluorescence lifetime of the acceptor emission at 630 nm in PSMA-M2 NPs was longer than that of bare-M2 NPs (Supporting Information Figure S9d), suggesting reduced self-quenching of the acceptor segments and consequently improved QY due to incorporation of PSMA matrix. A similar trend was observed by comparing the corresponding S1 and S2 samples.

Two-Photon Excitation Optical Properties. Two-photon excitation (2PE) optical properties of different PSMA-CP NPs in aqueous dispersion have been characterized by using femtosecond laser pulses with pulse duration of ~80 fs and repetition rate of 84.5 MHz (Figure 5). 2PE fluorescence

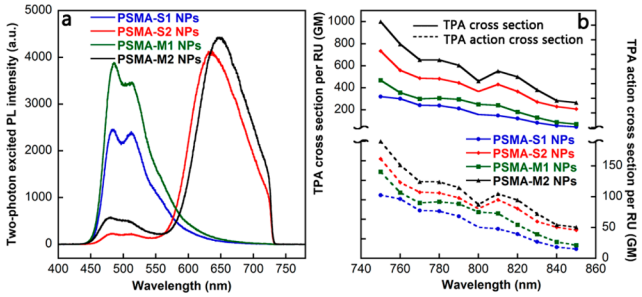

Figure 5. (a) 2PE fluorescence spectra of the PSMA-CP NPs with the same concentration (2.5 μM in RU) in water dispersion, λ_{EX} = 810 nm. (b) Wavelength dependent TPA cross section and two-photon action cross section values per repeat unit for different PSMA-CP NPs.

spectra of various PSMA-CP NPs (Figure 5a) are similar to their one-photon excitation fluorescence spectra (Figure 2f). 2PE fluorescence spectra of PSMA-M2 and PSMA-S2 displayed a minor donor emission band in the 450−550 nm range and a dominant acceptor emission band in the 600−700 nm range. Wavelength dependent TPA cross section and two-photon action cross section values per repeat unit for different PSMA-CP NPs from 750 to 850 nm have been measured by using Fluorescein in water (pH = 11) as the reference. All four CP NPs display largest TPA cross sections at 750 nm, the shortest excitation wavelength used in the experiment (the real TPA maximum could be located at even shorter wavelength beyond our measurement window). These results are summarized in Table 2. PSMA-S2 and PSMA-M2 NPs displayed much larger TPA cross sections than the corresponding undoped NPs (PSMA-S1 and PSMA-M1 NPs), which can be ascribed to formation of D-π-A-π-D structures in M2 and S2 by introduction of DTBT units. Formation of D-π-A-π-D

Table 2. Two-Photon Optical Properties of the PSMA-CP NPs in Aqueous Dispersion

PSMA-CP NPs	δ (GM)[a]	$\eta\delta$ (GM)[a]	δ (GM)[b]	$\eta\delta$ (GM)[b]
S1	320	102	3.1×10^4	1.0×10^4
S2	735	162	8.5×10^4	1.9×10^4
M1	469	141	3.9×10^4	1.2×10^4
M2	1000	190	2.5×10^5	4.7×10^4

[a]TPA cross section and two-photon action cross section per repeat unit at 750 nm. [b]TPA cross section and two-photon action cross section per NP at 750 nm.

structures facilitates the charge transfer between the donor moieties and π system of the molecule, resulting in larger electron delocalization and improved TPA cross sections.[42,55] PSMA-M2 NPs displayed larger TPA cross sections than PSMA-S2 NPs due to more planar π-electron conjugated systems of M2 (PSMA-M1 NPs displayed larger TPA cross section than PSMA-S1 NPs for the same reason). Among all four different PSMA-CP NPs, PSMA-M2 NPs displayed largest TPA cross sections, up to 1000 GM per RU at 750 nm. The corresponding two-photon action cross section reached 190 GM per RU. Considering one PSMA-M2 NP contains many molecules composed of many repeat units, TPA cross section and two-photon action cross section of M2 were estimated to be 2.5×10^5 and 4.7×10^4GM per nanoparticle, respectively. These conjugated polymer NPs have much higher δ and $\eta\delta$ values than the typical commercially available two-photon labeling agents, many previously reported QDs and organic dyes in water.[39,56−58] For example, the two-photon action cross section value of the PSMA-M2 NPs is about 7 times larger than that of QD655 ($\delta = 4.3 \times 10^4$ GM at 810 nm; $\eta = 15 \pm 2\%$),[58] and much higher than that of another commercial two-photon cell labeling agent, Evans Blue ($\delta_{max} \approx 150$ GM at 790 nm).[57]

Two-Photon Excitation Fluorescence Imaging of Cancer Cells. Large TPA action cross section of PSMA-CP NPs makes them attractive candidates as two-photon imaging agents. Good biocompatibility is a prerequisite for any bioimaging probes. The cytotoxicity of the PSMA-M1 and PSMA-M2 NPs were evaluated by monitoring the metabolic viability of $HepG_2$ cells after incubation with the NPs of different concentrations. Figure 6 shows that the cell viabilities remain nearly 100% after incubation with the NPs at 1.5 to 5 μM for 24 and 48 h, demonstrating their excellent

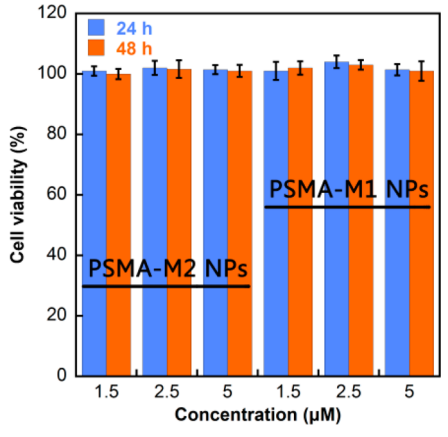

Figure 6. Metabolic viability of HepG2 cells after incubation with PSMA-M2 and PSMA-M1 NPs at different concentrations (in RU).

DOI: 10.1021/acsami.5b00223
ACS Appl. Mater. Interfaces 2015, 7, 6754−6763

biocompatibility. The concentrations of NPs in the viability test were much higher than that applied in the cell imaging experiments below to ensure their safe applications in biological imaging.

The application of PSMA-M2 NPs in 2PE cell imaging was demonstrated by using a laser scanning confocal microscope under femtosecond laser excitation at 750 nm. HepG2 cancer cells, HeLa cancer cells and NIH/3T3 cells were chosen as the model cell lines to test the application of these NPs as generic labeling agents (Supporting Information Figure S11). Three different NP concentrations (0.1, 0.5, and 2.5 μM) were used in the imaging experiments. The results shown that 0.5 μM of the NPs were sufficient to give clear cell images with high quality, which demonstrated high sensitivity of these NPs (Supporting Information Figure S12). 2PE fluorescence images of HepG2 cells after incubation with PSMA-M1 NPs and PSMA-M2 NPs are shown in Figure 7. Strong fluorescence was observed from

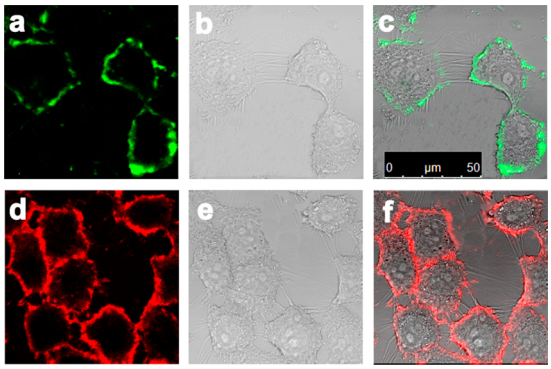

Figure 7. Two-photon excitation fluorescence images (a, d), bright-field images (b, e), and overlaid images (c, f) of HepG2 cancer cells after incubation with PSMA-M1 NPs (0.5 μM, a–c) and PSMA-M2 NPs (0.5 μM, d–f).

the cell membrane for all three types of cells, indicating that these PSMA-CP NPs are preferably located at the cell membrane. The preferential location of NPS at the cell membrane can be ascribed to favorable hydrophilic interactions between the carboxylic acid moiety of PSMA and the water molecules near the membrane lipid head groups, combined with the hydrophobic interactions between the aliphatic chains of the polymers and lipid molecules in the cell membrane.[59,60] As PSMA-M2 NPs emit red emission, which has much larger penetration depth than the green emission emitted by PSMA-M1NPs, much brighter 2PE cell images were obtained by using PSMA-M2 NPs as the probes than those using PSMA-M1 NPs. Furthermore, the cells without and after incubation with the NPs showed similar morphologies (Supporting Information Figure S13), which demonstrated little adverse effects of the NPs on the cell growth.

As a direct comparison with conventional imaging probes, cell imaging experiments of HepG2 cells after incubation with PSMA-M2 NPs and a commercial membrane tracker, CellMask Deep Red Plasma membrane stain, were performed under both one- and two-photon excitation (Figure 8). When PSMA-M2 NPs were used as the imaging probe, strong red fluorescence signals were observed from cell membrane to clearly distinguish the cell profile under both one- and two-photon excitation. In contrast, the cell imaging using CellMask Deep Red Plasma membrane stain only displayed detectable signals under one-photon excitation, while undetectable emission signals under

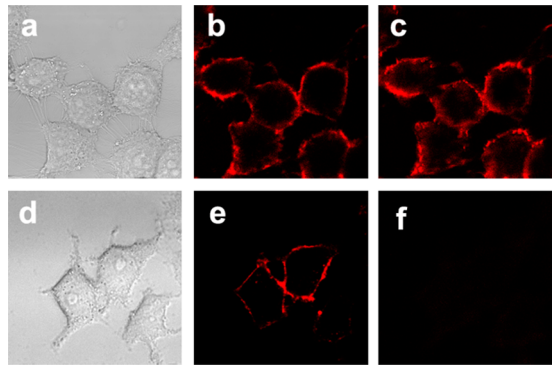

Figure 8. Bright-field images (left), one-photon excitation (middle), and two-photon (right) excitation images of HepG2 cells after incubation with PSMA-M2 NPs (top line) and CellMask Deep Red Plasma membrane stain (bottom line). Excitation wavelength is 405 (b), 650 (e), and 750 nm (c and f), respectively.

two-photon excitation because of its small TPA cross sections. These results highlight the advantages of these NPs over those commercial probes and their potential applications in both one- and two-photon excitation bioimaging. As plasma membrane is involved in a variety of important cellular processes such as cell adhesion and cell signaling, it is of high importance in biomedical research to develop new materials for membrane labeling and imaging of target living cells.[60−62] Considering these red emitting NPs could be further conjugated with specific targeting ligands or functional groups for targeted biological imaging, these polymer NPs hold great potentials as two-photon excitation fluorescence probes to take the full advantages of two-photon excitation for potential in vivo applications.

CONCLUSION

In summary, we have designed and synthesized two red emitting conjugated polymers (S2 and M2) based on incorporating classical TPA units-DPSB, electron-rich units-fluorene and a small amount of electron-deficient units-DTBT along the polymer backbones. Two green-emitting polymers (S1 and M1) without doping DTBT units were also synthesized as the control. Water-dispersible NPs based on these conjugated polymers were prepared using amphiphilic polymer PSMA as the encapsulation matrix. Strong red emission was obtained by FRET between the donor–acceptor pairs inside the NPs. The polymer/matrix ratio and the initial feed concentration of the polymer solution were optimized to achieve high red emission QYs of 24% and 19% for PSMA-S2 and PSMA-M2 NPs, respectively. Introduction of acceptor units DTBT into the polymer backbones forms the D-π-A-π-D structure, resulting in significantly enhanced TPA cross section. TPA cross section of S2 and M2 NPs were found to be 8.5×10^4 and 2.5×10^5 GM per NP in aqueous media. Owing to their large TPA cross section, high QY of red emission, excellent photostability and biocompatibility, the applications of these CP NPs as two-photon excitation fluorescence probes for cell membrane imaging with excellent imaging contrast have been demonstrated in three different cell lines. These polymer NPs hold great potentials as two-photon excitation fluorescence probes in various biological applications with potential of in vivo applications.

DOI: 10.1021/acsami.5b00223
ACS Appl. Mater. Interfaces 2015, 7, 6754–6763

EXPERIMENTAL SECTION

Characterization. ^{13}C NMR and ^{1}H NMR data were collected on a Bruker AVANCE Digital NMR workstation operating at 300 MHz. Chemical shifts were reported as δ value (ppm) relative to an internal tetramethylsilane (TMS) standard. Molecular weights of the polymers were determined by using a Waters 2410 gel permeation chromatograph (GPC) with a refractive index detector in THF using a calibration curve of polystyrene standards. Mass Spectrometry (MS) data were obtained on a WatersTQD with atmospheric pressure chemical ionization resource (APCI). UV−vis absorption and fluorescence spectra were measured by using a Shimadzu UV−vis spectrophotometer and a JobinYvon Fluoromax-4 spectrofluorometer, respectively. The fluorescence quantum yield of the polymers in THF and water were measured by using Fluorescein in aqueous solution (0.1 M NaOH; QY = 0.95) and Coumarin 153 in ethanol (QY = 0.53) as the standard. The absorbance of the solutions was kept below 0.1 to avoid internal filter effect. Average particle size and size distribution of the NPs were determined by dynamic light scattering (DLS) with a particle size analyzer (90 Plus, Brookhaven Instruments Co. USA) at room temperature. Transmission electron microscopic (TEM) images of the nanoparticles were recorded by using a JEOL 2010 microscope. Fluorescence lifetime measurements were performed on a TCSPC module from Picoquant GmbH (Berlin, Germany). The frequency-doubled output (410 nm, ∼ 30 μW) of an Avesta TiF-100 M femtosecond Ti:sapphire oscillator was used as the excitation source. The detector is a photomultiplier tubes (PMT) (PicoQuant) and has an instrument response function of 150 ps.

Materials. 4-(Diphenylamino)benzaldehyde(**1a**),[63] 4-((4-Bromophenyl)-phenylamino)benzaldehyde (**1b**),[63] 2,5-bis-(diethylphosphonatomethyl)-1,4-dibromobenzene (**2a**),[46] and tetraethyl-1,4-phenylenebis(methylene)diphosphonate (**2b**)[63] were synthesized from triphenylamine and 1,4-dimethylbenzene according to the previously reported methods. 2,7-Bis(4,4,5,5-tetramethyl-1,3,2-dioxaborolan-2-yl)-9,9-dioctylfluorene and 4,7-bis(5-bromo-2-thienyl)-2,1,3-benzothiadiazole were prepared according to the reported procedures.[64] Poly(styrene-*co*-maleic anhydride) (PSMA) was purchased from Sigma-Aldrich and used as received. THF was dried over Na/benzophenoneketyl and freshly distilled prior to use. The other materials were commercially available and used as received.

2,5-Bis(4-diphenylaminostyryl)-1,4-dibromobenzene (3a). **2a** (2.68 g, 5 mmol) was added to a solution of potassium *tert*-butoxide (1.68 g, 15 mmol) in dry THF (15 mL) at 0 °C, and then the mixture was stirred for 1 h. A solution of **1a** (3.00 g, 11 mmol) in dry THF was added via syringe, and the resulting mixture was then stirred at room temperature for 12 h. The reaction mixture was poured into water and extracted with CH_2Cl_2. The organic layer was washed with water, dried ($MgSO_4$), and concentrated under reduced pressure, recrystallization (CH_2Cl_2/hexane) afforded **3a** as a yellow solid (2.01 g, 52%).^{1}H NMR ($CDCl_3$, 300 MHz) δ = 7.83 (s, 2H), 7.41 (d, 4H), 7.28 (t, 4H), 7.26 (d, 4H), 7.24 (d, 2H), 7.13 (d, 8H), 7.06 (m, 8H), 7.00 ppm (d, 2H). ^{13}C NMR ($CDCl_3$, 300 MHz), d = 148.30, 147.55, 137.44, 131.71, 130.71, 130.20, 129.54, 128.05, 124.98, 124.08, 123.53, 123.24, 123.07 ppm. MS (APCI, *m*/*z*): calcd. For $C_{46}H_{34}Br_2N_2$ [M + 1]$^+$: 773.11; found, 772.12.

1,4-Bis(4-(4-Bromo-phenyl)-phenylaminostyryl)-benzene (3b). **2b** (1.89 g, 5 mmol) was added to a solution of potassium *tert*-butoxide (1.68 g, 15 mmol) in dry THF (15 mL) at 0 °C. The mixture was stirred for 1 h. A solution of **1b** (3.87 g, 11 mmol) in dry THF was added via syringe and the resulting mixture was then stirred at room temperature for 12 h. Some product had precipitated, the reaction mixture was then poured into lots of water, and the product was filtered. The solid material was recrystallized from large amounts of CH_2Cl_2 to give **3b** as a light yellow microcrystalline powder. (1.55 g, 41%).^{1}H NMR ($CDCl_3$, 300 MHz) δ = 7.47 (s, 4H), 7.41 (d, 2H), 7.38 (d, 2H), 7.35 (d, 2H), 7.32 (d, 2H), 7.27−7.24 (m, 6H), 7.11 (t, 2H), 7.08 (d, 2H), 7.05 (d, 4H), 7.02 (d, 4H), 6.99 (d, 2H), 6.96 ppm (d, 2H). ^{13}C NMR ($CDCl_3$, 300 MHz), δ = 148.51, 148.02, 146.42, 139.14, 132.43, 132.22, 129.86, 129.11, 128.43, 128.27, 127.55, 126.23, 125.07, 123.43, 123.05, 129.84, 124.91 ppm. MS (APCI, *m*/*z*): calcd. for $C_{46}H_{34}Br_2N_2$ [M + 1]$^+$: 773.11; found, 772.10.

Polymer S1. Compound **3a** (193.6 mg, 0.25 mmol), 2,7-bis(4,4,5,5-tetramethyl-1,3,2-dioxaborolan-2-yl)-9,9-dioctylfluorene (160.6 mg, 0.25 mmol) and $Pd(PPh_3)_4$(10 mg) were dissolved in toluene (5 mL). An aqueous K_2CO_3 solution (2 M, 2 mL) was added to the mixture under nitrogen atmosphere and the reaction mixture was degassed. The mixture was stirred at 85 °C for 24 h under nitrogen atmosphere. The reaction mixture was cooled to room temperature and poured into methanol (200 mL) to precipitate the resulting polymer. The resulting solid was filtered and dissolved in chloroform (20 mL). The solution was washed with water (300 mL) several times. The organic phase was separated and concentrated in vacuo to obtain the product in solid state, which was then purified by Soxhlet extraction with acetone. The polymer was extracted with chloroform followed by silica-gel chromatography with chloroform eluent. The polymer was reprecipitated using methanol and dried in vacuum at 60 °C overnight. Finally, polymer S1 was obtained as yellow solid (yield = 85%). GPC: M_n= 54.4 kDa, M_w = 124.2 kDa, PDI = 2.3.

Polymer S2. The synthetic method was similar to that of **S1** except that the starting material was **3a** (174.2 mg, 0.225 mmol), 4,7-bis(5-bromo-2-thienyl)-2,1,3-benzothiadiazole (11.5 mg, 0.025 mmol), 2,7-bis(4,4,5,5-tetramethyl-1,3,2-dioxaborolan-2-yl)-9,9-dioctylfluorene (160.6 mg, 0.25 mmol). **S2** was finally obtained as light red solid (yield = 83%). GPC: M_n = 52.3 kDa, M_w = 126.3 kDa, PDI = 2.4.

Polymer M1. The synthetic method was similar to that of **S1** except that the starting material were **3b** (193.6 mg, 0.25 mmol), 2,7-bis(4,4,5,5-tetramethyl-1,3,2-dioxaborolan-2-yl)-9,9-dioctylfluorene (160.6 mg, 0.25 mmol). The reaction time was only 2−3 h at 85 °C because of the much lower solubility of **M1.** Finally, polymer **M1** was obtained as yellow solid (yield = 63%). GPC: M_n = 29.1 kDa, M_w = 100.7 kDa, PDI = 3.4.

Polymer M2. The synthetic method was similar to that of **M1** except that the starting material were **3b** (174.2 mg, 0.225 mmol), 4,7-bis(5-bromo-2-thienyl)-2,1,3-benzothiadiazole (11.5 mg, 0.025 mmol), 2,7-bis(4,4,5,5-tetramethyl-1,3,2-dioxaborolan-2-yl)-9,9-dioctylfluorene (160.6 mg, 0.25 mmol). Finally, polymer **M2** was obtained as light red solid (yield = 62%). GPC: M_n = 27.2 kDa, M_w = 128.1 kDa, PDI = 4.7.

Preparation of PSMA Incorporated Polymer Nanoparticles (PSMA-CP NPs). PSMA-CP NPs were prepared using a modified reprecipitation method.[21] 24.0 μL of PSMA solution in THF (200 mM) were mixed with 2.0 mL of polymer stock solution in THF (10 μM). The mixtures were quickly added into 8 mL deionized water under sonication. THF was then removed by vacuum evaporation at 35 °C. PSMA-P NPs were obtained by filtration through a 0.22 μm filter. The bare NPs with no encapsulation matrix were prepared using the reprecipitation method similar to that of PSMA-P NPs except for not using any encapsulation matrix.

Two-Photon Excitation Fluorescence Measurements. 2PE fluorescence were measured by using an Avesta TiF-100 M femtosecond (fs) Ti:sapphire oscillator as the excitation source. The output laser pulses have pulse duration of ∼80 fs and a repetition rate of 84.5 MHz in the wavelength range from 750 to 850 nm. The laser beam was focused onto the sample that was contained in a cuvette with path length of 1 cm. The emission was collected at an angle of 90° to the incoming excitation beam by a pair of lenses and an optical fiber that was connected to a monochromator (Acton, Spectra Pro 2300i) coupled CCD (Princeton Instruments, Pixis 100B) system. A short pass filter with cutoff wavelength at 750 nm was placed before the spectrometer to minimize the scattering from the pump beam. Fluorescein in water (pH 11)[65] was used as reference (*r*). TPA cross section (δ) of the sample (s) at each wavelength can be calculated according to

$$\delta_S = \frac{I_s}{I_r} \cdot \frac{\varphi_r}{\varphi_s} \cdot \frac{C_r}{C_s} \cdot \delta_r$$

where *I* is the integrated 2PE fluorescence signals, φ is the fluorescence quantum yield, and *C* is concentration (in repeat unit for the

DOI: 10.1021/acsami.5b00223
ACS Appl. Mater. Interfaces 2015, 7, 6754−6763

polymer).[44] The uncertainty in the measurement of cross sections is ~15%.

Calculation of the Number (n) of Polymer Repeat Unit in NPs. The radius (r) of single CP NP was estimated based on the size results of DLS and TEM images (diameters of PSMA-CP NPs: S1−20 nm, S2−21 nm, M1−19 nm, M2−26 nm). The density (ρ) of the NP suspension could be roughly estimated to be ~1 g/cm^3.[62] The weight (m) of a single NP can be calculated by

$$m = V_\rho = \frac{4}{3}\pi r^3 \rho$$

where the units of m, r and ρ are g, cm, and g/cm^3, respectively. The number (n) of polymer repeat unit in a single polymer NP was calculated by

$$n = \frac{mA}{M} N_A = \frac{4\pi r^3 \rho A N_A}{3M}$$

where M, N_A, and A represent the repeat unit weight of polymer, Avogadro constant, and the weight ratio of the polymer in the NP, respectively.

Cell Culture. The human hepatocellular carcinoma cell line $HepG_2$ was cultured in growth media (DMEM supplemented with fetal bovine serum (10%), streptomycin (100.0 mg/L) and penicillin (100 IU/mL). Cells were maintained in a humidified atmosphere of 5% CO_2 at 37 °C.

Proliferation Assay. Cell viability was determined by using the XTT colorimetric cell proliferation kit (Roche) following the manufacturer's guidelines. Briefly, cells were grown to 20−30% confluence in 96-well plates. They will reach ~90% confluence within 24−48 h in the absence of compounds. The cells were treated with different concentrations of CP NPs, in triplicate, for 24 and 48 h, before the proliferation by the XTT assay.

Two-Photon Excitation Fluorescence Cell Imaging. $HepG_2$ cancer cells were seeded on glass bottom dishes (Mattek) and grown until 70−80% confluence. The PSMA-CP NPs (0.5 μM) were added into the medium and incubated for 2 h. After washing with the1 × PBS buffer solution, DMEM medium was added. The images were taken by using a Leica TCS SP5X confocal microscope system. A Ti-Sapphire oscillator with output femtosecond laser pulses at 750 nm was used as the two-photon excitation sources. Images were processed by using the Leica Application Suite Advanced Fluorescence (LAS AF) software.

■ ASSOCIATED CONTENT

Supporting Information

Detailed synthesis routes, TEM results, DLS results, fluorescence spectra of S1 and S2 samples, feed concentration dependent results of PSMA-M2 NPs, fluorescence stability, size stability, ζ-potential stability and photostability test results, fluorescence decay curves and lifetime fitting data, and cell imaging with different cell lines and concentration dependent cell imaging results. This material is available free of charge via the Internet at http://pubs.acs.org.

■ AUTHOR INFORMATION

Corresponding Authors

*E-mail: msfhuang@scut.edu.cn.
*E-mail: chmxqh@nus.edu.sg.

Notes

The authors declare no competing financial interest.

■ ACKNOWLEDGMENTS

We thank the financial support from the Ministry of Science and Technology (No. 2014CB643501), the Natural Science Foundation of China (Nos. 21125419 and 51361165301), the Guangdong Natural Science Foundation (No. S2012030006232), the Guangdong Innovative Research Team Program of China (201101C0105067115), and Faculty of Science, National University of Singapore (AcRF R-143-000-403-112).

■ REFERENCES

(1) Denk, W.; Strickler, J. H.; Webb, W. W. 2-Photon Laser Scanning Fluorescence Microscopy. *Science* **1990**, *248*, 73−76.
(2) Cahalan, M. D.; Parker, I.; Wei, S. H.; Miller, M. J. Two-Photon Tissue Imaging: Seeing the Immune System in a Fresh Light. *Nat. Rev. Immunol.* **2002**, *2*, 872−880.
(3) He, G. S.; Tan, L. S.; Zheng, Q.; Prasad, P. N. Multiphoton Absorbing Materials: Molecular Designs, Characterizations, and Applications. *Chem. Rev.* **2008**, *108*, 1245−1330.
(4) Kim, H. M.; Cho, B. R. Two-Photon Probes for Intracellular Free Metal Ions, Acidic Vesicles, and Lipid Rafts in Live Tissues. *Acc. Chem. Res.* **2009**, *42*, 863−872.
(5) Li, J. L.; Goh, C. C.; Keeble, J. L.; Qin, J. S.; Roediger, B.; Jain, R.; Wang, Y. L.; Chew, W. K.; Weninger, W.; Ng, L. G. Intravital Multiphoton Imaging of Immune Responses in the Mouse Ear Skin. *Nat. Protoc.* **2012**, *7*, 221−234.
(6) Albota, M.; Beljonne, D.; Bredas, J. L.; Ehrlich, J. E.; Fu, J. Y.; Heikal, A. A.; Hess, S. E.; Kogej, T.; Levin, M. D.; Marder, S. R.; McCord-Maughon, D.; Perry, J. W.; Rockel, H.; Rumi, M.; Subramaniam, C.; Webb, W. W.; Wu, X. L.; Xu, C. Design of Organic Molecules with Large Two-Photon Absorption Cross Sections. *Science* **1998**, *281*, 1653−1656.
(7) Larson, D. R.; Zipfel, W. R.; Williams, R. M.; Clark, S. W.; Bruchez, M. P.; Wise, F. W.; Webb, W. W. Water-Soluble Quantum Dots for Multiphoton Fluorescence Imaging in Vivo. *Science* **2003**, *300*, 1434−1436.
(8) Sánchez, S. A.; Gratton, E. Lipid−Protein Interactions Revealed by Two-Photon Microscopy and Fluorescence Correlation Spectroscopy. *Acc. Chem. Res.* **2005**, *38*, 469−477.
(9) Helmchen, F.; Denk, W. Deep Tissue Two-Photon Microscopy. *Nat. Methods* **2005**, *2*, 932−940.
(10) Roberts, W. G.; Palade, G. E. Increased Microvascular Permeability and Endothelial Fenestration Induced by Vascular Endothelial Growth-Factor. *J. Cell Sci.* **1995**, *108*, 2369−2379.
(11) Drobizhev, M.; Makarov, N. S.; Tillo, S. E.; Hughes, T. E.; Rebane, A. Two-Photon Absorption Properties of Fluorescent Proteins. *Nat. Methods* **2011**, *8*, 393−399.
(12) Smith, A. M.; Duan, H.; Mohs, A. M.; Nie, S. Bioconjugated Quantum Dots for in Vivo Molecular and Cellular Imaging. *Adv. Drug Delivery Rev.* **2008**, *60*, 1226−1240.
(13) Medintz, I. L.; Uyeda, H. T.; Goldman, E. R.; Mattoussi, H. Quantum Dot Bioconjugates for Imaging, Labelling and Sensing. *Nat. Mater.* **2005**, *4*, 435−446.
(14) Resch-Genger, U.; Grabolle, M.; Cavaliere-Jaricot, S.; Nitschke, R.; Nann, T. Quantum Dots Versus Organic Dyes as Fluorescent Labels. *Nat. Methods* **2008**, *5*, 763−775.
(15) Wu, C.; Schneider, T.; Zeigler, M.; Yu, J.; Schiro, P. G.; Burnham, D. R.; McNeill, J. D.; Chiu, D. T. Bioconjugation of Ultrabright Semiconducting Polymer Dots for Specific Cellular Targeting. *J. Am. Chem. Soc.* **2010**, *132*, 15410−15417.
(16) Li, K.; Ding, D.; Huo, D.; Pu, K.-Y.; Thao, N. N. P.; Hu, Y.; Li, Z.; Liu, B. Conjugated Polymer Based Nanoparticles as Dual-Modal Probes for Targeted in Vivo Fluorescence and Magnetic Resonance Imaging. *Adv. Funct. Mater.* **2012**, *22*, 3107−3115.
(17) Pu, K.-Y.; Liu, B. Fluorescent Conjugated Polyelectrolytes for Bioimaging. *Adv. Funct. Mater.* **2011**, *21*, 3408−3423.
(18) Wu, C.; Chiu, D. T. Highly Fluorescent Semiconducting Polymer Dots for Biology and Medicine. *Angew. Chem., Int. Ed.* **2013**, *52*, 3086−109.
(19) Shen, X. Q.; He, F.; Wu, J. H.; Xu, G. Q.; Yao, S. Q.; Xu, Q. H. Enhanced Two-Photon Singlet Oxygen Generation by Photosensitizer-Doped Conjugated Polymer Nanoparticles. *Langmuir* **2011**, *27*, 1739−1744.

DOI: 10.1021/acsami.5b00223
ACS Appl. Mater. Interfaces 2015, 7, 6754−6763

(20) Wu, C. F.; Peng, H. S.; Jiang, Y. F.; McNeill, J. Energy Transfer Mediated Fluorescence from Blended Conjugated Polymer Nanoparticles. *J. Phys. Chem. B* **2006**, *110*, 14148−14154.
(21) Shen, X.; Li, L.; Wu, H.; Yao, S. Q.; Xu, Q. H. Photosensitizer-Doped Conjugated Polymer Nanoparticles for Simultaneous Two-Photon Imaging and Two-Photon Photodynamic Therapy in Living Cells. *Nanoscale* **2011**, *3*, 5140−6.
(22) Feng, X.; Liu, L.; Wang, S.; Zhu, D. Water-Soluble Fluorescent Conjugated Polymers and Their Interactions with Biomacromolecules for Sensitive Biosensors. *Chem. Soc. Rev.* **2010**, *39*, 2411−2419.
(23) Zhu, C.; Liu, L.; Yang, Q.; Lv, F.; Wang, S. Water-Soluble Conjugated Polymers for Imaging, Diagnosis, and Therapy. *Chem. Rev.* **2012**, *112*, 4687−735.
(24) Wu, C.; Bull, B.; Szymanski, C.; Christensen, K.; McNeill, J. Multicolor Conjugated Polymer Dots for Biological Fluorescence Imaging. *ACS Nano* **2008**, *2*, 2415−2423.
(25) Ding, D.; Li, K.; Qin, W.; Zhan, R.; Hu, Y.; Liu, J.; Tang, B. Z.; Liu, B. Conjugated Polymer Amplified Far-Red/near-Infrared Fluorescence from Nanoparticles with Aggregation-Induced Emission Characteristics for Targeted in Vivo Imaging. *Adv. Healthcare Mater.* **2013**, *2*, 500−507.
(26) Wu, W.-C.; Chen, C.-Y.; Tian, Y.; Jang, S.-H.; Hong, Y.; Liu, Y.; Hu, R.; Tang, B. Z.; Lee, Y.-T.; Chen, C.-T.; Chen, W.-C.; Jen, A. K. Y. Enhancement of Aggregation-Induced Emission in Dye-Encapsulating Polymeric Micelles for Bioimaging. *Adv. Funct. Mater.* **2010**, *20*, 1413−1423.
(27) Liu, J.; Feng, G.; Ding, D.; Liu, B. Bright Far-Red/Near-Infrared Fluorescent Conjugated Polymer Nanoparticles for Targeted Imaging of Her2-Positive Cancer Cells. *Polym. Chem.* **2013**, *4*, 4326−4334.
(28) Thomas, S. W.; Joly, G. D.; Swager, T. M. Chemical Sensors Based on Amplifying Fluorescent Conjugated Polymers. *Chem. Rev.* **2007**, *107*, 1339−1386.
(29) Wu, C.; Hansen, S. J.; Hou, Q.; Yu, J.; Zeigler, M.; Jin, Y.; Burnham, D. R.; McNeill, J. D.; Olson, J. M.; Chiu, D. T. Design of Highly Emissive Polymer Dot Bioconjugates for in Vivo Tumor Targeting. *Angew. Chem., Int. Ed.* **2011**, *50*, 3430−4.
(30) Chan, Y.-H.; Ye, F.; Gallina, M. E.; Zhang, X.; Jin, Y.; Wu, I. C.; Chiu, D. T. Hybrid Semiconducting Polymer Dot−Quantum Dot with Narrow-Band Emission, near-Infrared Fluorescence, and High Brightness. *J. Am. Chem. Soc.* **2012**, *134*, 7309−7312.
(31) Wu, C.; Bull, B.; Christensen, K.; McNeill, J. Ratiometric Single-Nanoparticle Oxygen Sensors for Biological Imaging. *Angew. Chem., Int. Ed.* **2009**, *48*, 2741−2745.
(32) Liu, J.; Geng, J.; Liu, B. A Bright Far-Red and near-Infrared Fluorescent Conjugated Polyelectrolyte with Quantum Yield Reaching 25%. *Chem. Commun.* **2013**, *49*, 1491−1493.
(33) Ding, D.; Liu, J.; Feng, G.; Li, K.; Hu, Y.; Liu, B. Bright Far-Red/Near-Infrared Conjugated Polymer Nanoparticles for in Vivo Bioimaging. *Small* **2013**, *9*, 3093−102.
(34) Chen, C.-Y.; Tian, Y.; Cheng, Y.-J.; Young, A. C.; Ka, J.-W.; Jen, A. K. Y. Two-Photon Absorbing Block Copolymer as a Nanocarrier for Porphyrin: Energy Transfer and Singlet Oxygen Generation in Micellar Aqueous Solution. *J. Am. Chem. Soc.* **2007**, *129*, 7220−7221.
(35) Geng, J.; Zhu, Z.; Qin, W.; Ma, L.; Hu, Y.; Gurzadyan, G. G.; Tang, B. Z.; Liu, B. Near-Infrared Fluorescence Amplified Organic Nanoparticles with Aggregation-Induced Emission Characteristics for in Vivo Imaging. *Nanoscale* **2014**, *6*, 939−945.
(36) So, P. T. C.; Dong, C. Y.; Masters, B. R.; Berland, K. M. Two-Photon Excitation Fluorescence Microscopy. *Annu. Rev. Biomed. Eng.* **2000**, *2*, 399−429.
(37) Ji, N.; Magee, J. C.; Betzig, E. High-Speed, Low-Photodamage Nonlinear Imaging Using Passive Pulse Splitters. *Nat. Methods* **2008**, *5*, 197−202.
(38) Zhu, M. Q.; Zhang, G. F.; Li, C.; Aldred, M. P.; Chang, E.; Drezek, R. A.; Li, A. D. Q. Reversible Two-Photon Photoswitching and Two-Photon Imaging of Immunofunctionalized Nanoparticles Targeted to Cancer Cells. *J. Am. Chem. Soc.* **2011**, *133*, 365−372.
(39) Shen, X.; Li, L.; Min Chan, A. C.; Gao, N.; Yao, S. Q.; Xu, Q.-H. Water-Soluble Conjugated Polymers for Simultaneous Two-Photon Cell Imaging and Two-Photon Photodynamic Therapy. *Adv. Opt. Mater.* **2013**, *1*, 92−99.
(40) Guan, Z.; Polavarapu, L.; Xu, Q. H. Enhanced Two-Photon Emission in Coupled Metal Nanoparticles Induced by Conjugated Polymers. *Langmuir* **2010**, *26*, 18020−3.
(41) Hrobarikova, V.; Hrobarik, P.; Gajdos, P.; Fitilis, I.; Fakis, M.; Persephonis, P.; Zahradnik, P. Benzothiazole-Based Fluorophores of Donor-π-Acceptor-π-Donor Type Displaying High Two-Photon Absorption. *J. Org. Chem.* **2010**, *75*, 3053−68.
(42) Pond, S. J. K.; Rumi, M.; Levin, M. D.; Parker, T. C.; Beljonne, D.; Day, M. W.; Bredas, J. L.; Marder, S. R.; Perry, J. W. One- and Two-Photon Spectroscopy of Donor-Acceptor-Donor Distyrylbenzene Derivatives: Effect of Cyano Substitution and Distortion from Planarity. *J. Phys. Chem. A* **2002**, *106*, 11470−11480.
(43) Pawlicki, M.; Collins, H. A.; Denning, R. G.; Anderson, H. L. Two-Photon Absorption and the Design of Two-Photon Dyes. *Angew. Chem., Int. Ed.* **2009**, *48*, 3244−66.
(44) Tian, Y.; Chen, C. Y.; Cheng, Y. J.; Young, A. C.; Tucker, N. M.; Jen, A. K. Y. Hydrophobic Chromophores in Aqueous Micellar Solution Showing Large Two-Photon Absorption Cross Sections. *Adv. Funct. Mater.* **2007**, *17*, 1691−1697.
(45) Woo, H. Y.; Korystov, D.; Mikhailovsky, A.; Nguyen, T.-Q.; Bazan, G. C. Two-Photon Absorption in Aqueous Micellar Solutions. *J. Am. Chem. Soc.* **2005**, *127*, 13794−13795.
(46) Huang, F.; Tian, Y.; Chen, C.-Y.; Cheng, Y.-J.; Young, A. C.; Jen, A. K. Y. Cross-Conjugated Polymers with Large Two-Photon Absorption Cross-Sections for Metal Ion Sensing. *J. Phys. Chem. C* **2007**, *111*, 10673−10681.
(47) Starkey, J. R.; Rebane, A. K.; Drobizhev, M. A.; Meng, F.; Gong, A.; Elliott, A.; McInnerney, K.; Spangler, C. W. New Two-Photon Activated Photodynamic Therapy Sensitizers Induce Xenograft Tumor Regressions after near-IR Laser Treatment through the Body of the Host Mouse. *Clin. Cancer Res.* **2008**, *14*, 6564−6573.
(48) Frederiksen, P. K.; Jorgensen, M.; Ogilby, P. R. Two-Photon Photosensitized Production of Singlet Oxygen. *J. Am. Chem. Soc.* **2001**, *123*, 1215−1221.
(49) Qin, T.; Zajaczkowski, W.; Pisula, W.; Baumgarten, M.; Chen, M.; Gao, M.; Wilson, G.; Easton, C. D.; Mullen, K.; Watkins, S. E. Tailored Donor−Acceptor Polymers with an a-D1−a-D2 Structure: Controlling Intermolecular Interactions to Enable Enhanced Polymer Photovoltaic Devices. *J. Am. Chem. Soc.* **2014**, *136*, 6049−55.
(50) Wu, C. F.; Szymanski, C.; McNeill, J. Preparation and Encapsulation of Highly Fluorescent Conjugated Polymer Nanoparticles. *Langmuir* **2006**, *22*, 2956−2960.
(51) Turro, N. J.; Barton, J. K.; Tomalia, D. A. Molecular Recognition and Chemistry in Restricted Reaction Spaces. Photophysics and Photoinduced Electron Transfer on the Surfaces of Micelles, Dendrimers, and DNA. *Acc. Chem. Res.* **1991**, *24*, 332−340.
(52) Feng, G.; Li, K.; Liu, J.; Ding, D.; Liu, B. Bright Single-Chain Conjugated Polymer Dots Embedded Nanoparticles for Long-Term Cell Tracing and Imaging. *Small* **2014**, *10*, 1212−9.
(53) Li, K.; Qin, W.; Ding, D.; Tomczak, N.; Geng, J.; Liu, R.; Liu, J.; Zhang, X.; Liu, H.; Liu, B.; Tang, B. Z. Photostable Fluorescent Organic Dots with Aggregation-Induced Emission (AIE Dots) for Noninvasive Long-Term Cell Tracing. *Sci. Rep.* **2013**, *3*, 1150.
(54) Patterson, G. H.; Piston, D. W. Photobleaching in Two-Photon Excitation Microscopy. *Biophys. J. .* **2000**, *78*, 2159−2162.
(55) Albota, M.; Beljonne, D.; Brédas, J.-L.; Ehrlich, J. E.; Fu, J.-Y.; Heikal, A. A.; Hess, S. E.; Kogej, T.; Levin, M. D.; Marder, S. R.; McCord-Maughon, D.; Perry, J. W.; Röckel, H.; Rumi, M.; Subramaniam, G.; Webb, W. W.; Wu, X.-L.; Xu, C. Design of Organic Molecules with Large Two-Photon Absorption Cross Sections. *Science* **1998**, *281*, 1653−1656.
(56) Zhao, Z.; Chen, B.; Geng, J.; Chang, Z.; Aparicio-Ixta, L.; Nie, H.; Goh, C. C.; Ng, L. G.; Qin, A.; Ramos-Ortiz, G.; Liu, B.; Tang, B. Z. Red Emissive Biocompatible Nanoparticles from Tetraphenylethene-Decorated Bodipy Luminogens for Two-Photon Excited Fluorescence Cellular Imaging and Mouse Brain Blood Vascular Visualization. *Part. Part. Syst. Charact.* **2014**, *31*, 481−491.

DOI: 10.1021/acsami.5b00223
ACS Appl. Mater. Interfaces 2015, 7, 6754−6763

(57) Geng, J.; Goh, C. C.; Tomczak, N.; Liu, J.; Liu, R.; Ma, L.; Ng, L. G.; Gurzadyan, G. G.; Liu, B. Micelle/Silica Co-Protected Conjugated Polymer Nanoparticles for Two-Photon Excited Brain Vascular Imaging. *Chem. Mater.* **2014**, *26*, 1874−1880.
(58) Ding, D.; Goh, C. C.; Feng, G.; Zhao, Z.; Liu, J.; Liu, R.; Tomczak, N.; Geng, J.; Tang, B. Z.; Ng, L. G.; Liu, B. Ultrabright Organic Dots with Aggregation-Induced Emission Characteristics for Real-Time Two-Photon Intravital Vasculature Imaging. *Adv. Mater.* **2013**, *25*, 6083−6088.
(59) Kim, H. M.; Kim, B. R.; Choo, H. J.; Ko, Y. G.; Jeon, S. J.; Kim, C. H.; Joo, T.; Cho, B. R. Two-Photon Fluorescent Probes for Biomembrane Imaging: Effect of Chain Length. *ChemBioChem.* **2008**, *9*, 2830−2838.
(60) Li, L.; Shen, X. Q.; Xu, Q. H.; Yao, S. Q. A Switchable Two-Photon Membrane Tracer Capable of Imaging Membrane-Associated Protein Tyrosine Phosphatase Activities. *Angew. Chem., Int. Ed.* **2013**, *52*, 424−428.
(61) Dahan, M.; Lévi, S.; Luccardini, C.; Rostaing, P.; Riveau, B.; Triller, A. Diffusion Dynamics of Glycine Receptors Revealed by Single-Quantum Dot Tracking. *Science* **2003**, *302*, 442−445.
(62) Liu, J.; Feng, G.; Liu, R.; Tomczak, N.; Ma, L.; Gurzadyan, G. G.; Liu, B. Bright Quantum-Dot-Sized Single-Chain Conjugated Polyelectrolyte Nanoparticles: Synthesis, Characterization and Application for Specific Extracellular Labeling and Imaging. *Small* **2014**, *10*, 3110−3118.
(63) Wang, H.-Y.; Chen, G.; Xu, X.-P.; Chen, H.; Ji, S.-J. The Synthesis and Photophysical Properties of Novel Poly(Diarylamino)-Styrenes. *Dyes Pigm.* **2011**, *88*, 358−365.
(64) Hou, Q.; Xu, Y.; Yang, W.; Yuan, M.; Peng, J.; Cao, Y. Novel Red-Emitting Fluorene-Based Copolymers. *J. Mater. Chem.* **2002**, *12*, 2887−2892.
(65) Xu, C.; Webb, W. W. Measurement of Two-Photon Excitation Cross Sections of Molecular Fluorophores with Data from 690 to 1050 nm. *J. Opt. Soc. Am. B* **1996**, *13*, 481−491.

DOI: 10.1021/acsami.5b00223
ACS Appl. Mater. Interfaces 2015, 7, 6754−6763